

## RADIOCARBON AGES OF PLANT REMAINS IN MASSIVE GROUND ICE AND UNDERLYING SEDIMENTS OF THE BARROW PERMAFROST TUNNEL, ALASKA

Go Iwahana<sup>1\*</sup>  • Masao Uchida<sup>2</sup>  • Kazuho Horiuchi<sup>3</sup> • Jody Deming<sup>4</sup> • Hajo Eicken<sup>1</sup> • Hiroshi Ohno<sup>5</sup> • Kanako Mantoku<sup>2</sup> • Toshiyuki Kobayashi<sup>2</sup> • Kazuyuki Saito<sup>6</sup>

<sup>1</sup>International Arctic Research Center, University of Alaska Fairbanks, 2160 Koyukuk Drive, Fairbanks, AK 99775, USA

<sup>2</sup>Earth System Division, National Institute for Environmental Studies, Japan

<sup>3</sup>Graduate School of Science and Technology, Hirosaki University, Japan

<sup>4</sup>School of Oceanography, University of Washington, Seattle, WA, USA

<sup>5</sup>Kitami Institute of Technology, Japan

<sup>6</sup>Japan Agency for Marine-Earth Science and Technology, Japan

**ABSTRACT.** Massive ground ice found in the Barrow Permafrost Tunnel at 3–7 m depths from the surface has been interpreted as an ice wedge and used to reconstruct early Holocene environmental changes. To better understand the development of this ground ice, we conducted radiocarbon dating for 34 samples of plant remains from the massive ground ice and underlying sediment layer. A significantly large gap in the measured radiocarbon ages (more than 24 ka) between massive ice and the underlying sediment layer throughout the tunnel profile suggested at least two possibilities. One is that the lower and older sediment layer had thrust upwards at the boundary between intruding ice wedge and adjacent sediment, and the growing ice had pushed the sediment sideways. Another is that erosional events had removed surface materials at about 12–36 ka BP (14–41 cal ka BP) before the overlaying sediment layer with massive ground ice developed. The overall distribution of radiocarbon ages from the massive ice supported the ice-wedge hypothesis as a formation mechanism, although our results showed several age inversions and large fluctuations. Dating of densely spaced samples revealed two ground-ice regions with similar ages around 11–11.5 and 10–10.5 ka BP divided by a relatively narrow region of transitional ages along the tunnel long-axis. This distribution may be explained by a possible misalignment between the sampling direction and the ice-wedge growth line or by intermittent ice growth with repeated cracking at more random locations than the classic ice-wedge growth model suggested.

**KEYWORDS:** Barrow Permafrost Tunnel, ice wedge, massive ground ice, permafrost.

### INTRODUCTION

Ground ice has been used to study past environmental and developmental history through its geochemistry, ground-ice structure (cryostructure), and relationship to the host deposits (Gilbert et al. 2016). Using ground ice as a paleoclimate proxy is especially important for studies in periglacial areas where paleo-records from ice cores, lake sediments, and tree rings are less available or absent in the vicinity. In contrast to glacial ice core records that commonly integrate annual climate signals and summer-biased lake sediment records, the permafrost archive preserves both summer-specific (floral and faunal fossils) and winter-specific (ice wedge) information (Wetterich et al. 2021). The classic growth model of ice wedges includes the annually repeated opening of thermal contraction cracks in the winter permafrost ground, followed by compaction of snow/hoarfrost and infiltration of spring snowmelt and refreezing of water in perennially frozen layers (Leffingwell 1915; Lachenbruch 1962; Mackay 1990; St-Jean et al. 2011; Boereboom et al. 2013). If repeated cracking occurs at the center of an ice wedge, it grows symmetrically in the direction perpendicular to the crack line (Mackay 1974). The wedge ice consists of winter precipitation, with the youngest and oldest ices occurring, respectively, in the center and edges of the ice wedge. Although this idealized cracking pattern

\*Corresponding author. Email: [giwahana@alaska.edu](mailto:giwahana@alaska.edu)

has seldom been observed, ice wedges have been used as archives of winter paleoclimate (Meyer et al. 2015; Opel et al. 2018).

The Barrow Permafrost Tunnel is located near the town of Utqiagvik and is a unique facility that provides access to massive ground ice distributed at depths of about 3–7 m and enables three-dimensional sampling of permafrost. Cold Regions Research and Engineering Laboratory excavated the tunnel for permafrost study in 1962 (Brown 1969; Brown 1980). The tunnel was created within the massive ground ice, with the dimension of the adit space being about 10 m long and 1.5 m wide (Figure 2).

Using permafrost samples from this tunnel, several studies were conducted. Meyer et al. (2010a; 2010b) analyzed past environmental history using spatially sampled permafrost in the tunnel. Their research indicated that the massive ground ice in the tunnel developed as an ice wedge during the Late Glacial–Early Holocene (10–12 ka BP), recording winter climate information. Iizuka et al. (2019) conducted high-resolution sampling for ion concentration analysis in the ground ice along the Meyer et al. sampling transect. They found a high methanesulfonate ion concentration through the beginning of the Younger Dryas (YD) period, suggesting the existence of a nearby open sea surface during the coldest YD periods. A unique occurrence of cryopeg brines was found in this tunnel (Iwahana et al. 2021), and the microbiology of the brines was reported by Colangelo-Lillis et al. (2016), Cooper et al. (2019), Zhong et al. (2020), and Rapp et al. (2021).

To better constrain the age of permafrost development in the tunnel and to better interpret and understand the geochemistry information from the samples collected, we conducted additional radiocarbon dating for newly collected macro-plant remains obtained from the massive ground ice in the tunnel and underlying sediment layers. The objective of this paper is to evaluate the origin and developmental history of the permafrost surrounding the Barrow Permafrost Tunnel with the new dating information.

## MATERIALS AND METHODS

Permafrost (including massive ground ice and frozen sediments) samples were collected in the Barrow Permafrost Tunnel (71.294°N, 156.715°W; Figure 1) at a depth of about 5 m from the ground surface on several occasions from 2016 to 2018. Using electrical chain saws, fifteen block samples in the shape of triangular prisms were cut out along the A–A' transect of Meyer et al. (2010a). Our sampling line was 6.2 m long and about 0.3–0.5 m below the Meyer et al. sampling scars and about 0.5 m above the tunnel floor.

A cordless electrical drill with various types of corers (including US Snow, Ice, and Permafrost Research Establishment—SIPRE—corer manufactured by Jon's Machine Shop, Fox, Alaska) was used to sample cores of the permafrost below the tunnel floor. We cleaned the sampling tools before every sampling to avoid cross-contamination between sampling points. Details of the sampling procedure and observations in boreholes are described in supplemental texts S2 and S3 of Iwahana et al. (2021). Collected massive ice and frozen sediments were labeled, packed, and kept frozen until further subsampling and analysis in the laboratory at the University of Alaska Fairbanks (UAF).

The radiocarbon ages of macro-plant remains (moss, fine roots, leaves, or twigs) found in the sampled ground ice or sediments were determined by Accelerator Mass Spectrometry (AMS) laboratories of the University of Arizona, USA, and National Institute for Environmental

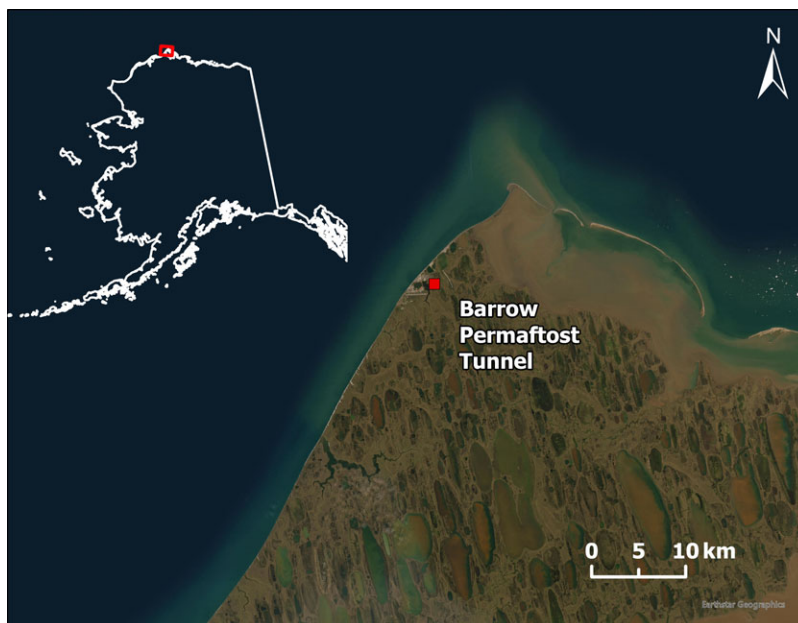


Figure 1 Location of the Barrow Permafrost Tunnel.

Studies, Japan (Uchida et al. 2005; Uchida et al. 2023). The macro-plant remains used for the measurements were collected from freeze-dried samples. The collected plant remains were washed with distilled water to avoid the influence of small particulates of organic carbon on radiocarbon measurements. The measured radiocarbon ages were calibrated using the OxCal (v4.4.4) software (Ramsey 2009) and IntCal20 atmospheric curve (Reimer et al. 2020). Radiocarbon ages obtained in this study are listed in uncalibrated BP and calibrated BP in Table 1. Uncalibrated BP was used in the following text and figures because ages of plant remains in permafrost often cannot be regarded as sedimentation ages in permafrost studies, as discussed in the Results and Discussion below. We used both uncalibrated BP and calibrated BP when discussing sedimentation rates and the environment in the past for a purpose of simple comparisons.

## RESULTS AND DISCUSSION

### Age Unconformity between Massive Ground Ice and Underlying Sediments

Significantly older ages (36 ka BP and older than 48 ka BP) were determined for plant remains found in the sediment layer immediately underneath the massive ground ice in the tunnel (Table 1; Figure 2). Considering the range of radiocarbon ages (9.9–12.4 ka BP) determined from plant remains in the massive ground ice (Figures 2 and 3), there is a significant gap (more than 24 ka) between the ages of the massive ground ice (Unit II) and underlying sediments (Unit I or bottom of Unit II).

The observed age unconformity is somewhat reasonable if the ice-wedge model is assumed for the mechanism of massive ground ice formation. Repeated winter cracking and surface water infiltration can introduce newer organic matter into the older sediment layers. Assuming the classic ice-wedge model, then Unit II sediment, which had been overlaying Unit I before the

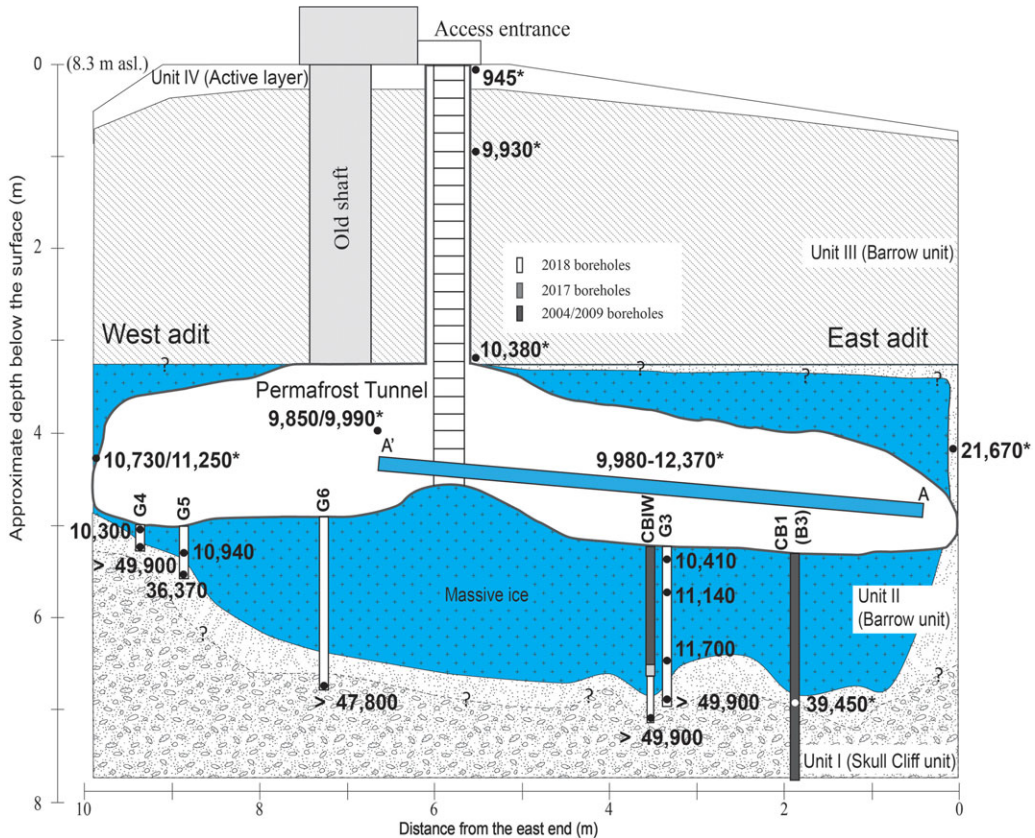


Figure 2 Cross section of the Barrow Permafrost Tunnel and sampling locations. Radiocarbon dates of the macro-plant remains sampled at the dot locations are displayed in uncalibrated BP. For transect A'-A, a range of the measured radiocarbon ages is displayed. Values with asterisks are from Meyer et al. (2010a).

ice-wedge formation, had been scraped away towards the edges of the ice wedge, or as in this study, towards the ends of the tunnel at the depth of Unit II (see Iwahana et al. 2021; Meyer et al. 2010a for Unit descriptions).

Unit I, the lowermost layer, consists of dark-gray silt and gravelly fine- to medium-grained sand and harbors cryopeg occurrences (Iwahana et al. 2021). Unit I is associated with the Skull Cliff unit, which was influenced by the Pelukian Transgression (Hopkins, 1967; Brigham-Grette and Hopkins, 1995), which has been associated with the last interglacial “Eemian” or Marine Isotope Stage (MIS) 5e. The age range of the Pelukian Transgression was recently dated as between 113 and 71 ka BP (Farquharson et al. 2018). Unit I was also influenced more recently by the last major transgression, the Simpsonian transgression (Dinter et al. 1990; Brigham-Grette and Hopkins 1995), which occurred between 53 and 81 ka BP (Carter et al. 1986). The Pelukian Transgression submerged the Utqiagvik region and formed a relict barrier-island system (Pelukian barrier-island system) 6–10 m above sea level, in which the studied tunnel is located.

Unit II overlays Unit I and is associated with the Barrow unit. The unit contains poorly sorted fine-grained yellowish-grey sandy silt sediments and massive ice portions with organic matter

Table 1 Radiocarbon dating of macro-plant remains in the massive ground ice and underlying sediments of the Barrow Permafrost Tunnel. Samples with asterisks were measured by Meyer et al. (2010a).

Sample type	ID	Distance from point A [m]	Depth from tunnel floor [m]	$^{14}\text{C}$ age [BP]	Calibrated age range ( $2\sigma$ ) [cal BP]	Mean [cal BP]	Lab#
Wall ice	A3	1.00		11260 ±30	13,240 13,090	13,165	AA109134-B10600
	A4-1	1.22		10150 ±60	11,970 11,400	11,685	TERRA-042518a21
	A4-3	1.41		11470 ±50	13,470 13,190	13,330	TERRA-042518a19
	A5	1.83		11070 ±50	13,100 12,840	12,970	TERRA-042518a18
	A6-C	2.34		10990 ±50	13,080 12,760	12,920	TERRA-042518a16
	A6-4	2.44		10830 ±50	12,880 12,720	12,800	TERRA-042418a18
	A6-2	2.50		11500 ±30	13,460 13,300	13,380	AA109135-B10601
	A6-5	2.55		11300 ±30	13,300 13,110	13,205	AA110948-X32644
	A7-1	2.63		11250 ±30	13,230 13,090	13,160	AA110950-X32646
	A7	2.78		11,070 ±30	13,100 12,900	13,000	AA110949-X32645
	A7-3	2.83		11,220 ±40	13,180 13,090	13,135	AA110951-X32647
	A'8	3.00		11,450 ±30	13,440 13,230	13,335	AA109136-B10602
	A'8-1	3.03		10,730 ±30	12,750 12,690	12,720	AA110959-X32655
	A'7-2	3.29		10,490 ±30	12,630 12,200	12,415	AA110958-X32654
	A'7-1	3.49		10,710 ±30	12,750 12,680	12,715	AA110956-X32652
	A'6-3	3.80		9,990 ±50	11,710 11,260	11,485	TERRA-042518a15
	A'6-C	4.00		10,120 ±30	11,880 11,400	11,640	AA109137-B10603
	A'6	4.01		10,320 ±33	12,460 11,940	12,200	AA110955-X32651
	A'5	4.27		9,980 ±40	11,690 11,260	11,475	TERRA-042518a17
	A'4	4.71		10,030 ±40	11,750 11,320	11,535	TERRA-042518a14
	A'3	5.11		10,260 ±30	12,430 11,820	12,125	AA110954-X32650
	A'2	5.50		10,300 ±50	12,460 11,830	12,145	AA109138-B10604
	A'1-4	5.83		10,340 ±30	12,470 11,950	12,210	AA110953-X32649
	A'1	6.10		10,360 ±50	12,480 11,970	12,225	AA110952-X32648

(Continued)

Table 1 (Continued)

Sample type	ID	Distance from point A [m]	Depth from tunnel floor [m]	<sup>14</sup> C age [BP]	Calibrated age range (2σ) [cal BP]	Mean [cal BP]	Lab#		
Floor ice	G3-Ia	2.9	0.16	10,410 ±30	12,580	12,050	12,315	TERRA-03123a7	
	G3-Ib	2.9	0.69	11,140 ±30	13,160	12,920	13,040	TERRA-03123a8	
	G3-Ic	2.9	1.38	11,700 ±40	13,740	13,460	13,600	AA113305-X34961	
	G5-I	8.4	0.28	10,940 ±80	13,070	12,740	12,905	AA113308-X34964	
	G4-I	8.9	0.08	10,300 ±30	12,450	11,880	12,165	TERRA-03123a9	
Sediment	G3-S	2.9	1.72	>49,900	–	–	–	AA113306-X34962	
	CBIW-S	3	1.91	>49,900	–	–	–	AA113307-X34963	
	G6-S	6.8	1.87	>47,800	–	–	–	AA114315-X35909	
	G5-S	8.4	0.52	36,370 ±760	42,290	40,090	41,190	AA113309-X34965	
	G4-S	8.9	0.27	>49,900	–	–	–	AA114314-X35908	
				Depth from ground surface [m]					
		S_0.15*		0.15	945 ±40	930	740	835	KIA25273
		S_0.95*		0.95	9,930 ±40	11,610	11,230	11,420	KIA24874
		S_3.45*		3.45	10,380 ±40	12,480	12,000	12,240	KIA24875
		S_4.10*		4.1	21,670 ±500	27,170	25,010	26,090	KIA24876
	S_6.80*		6.8	39,450 ±1180	45,070	41,970	43,520	KIA31129	

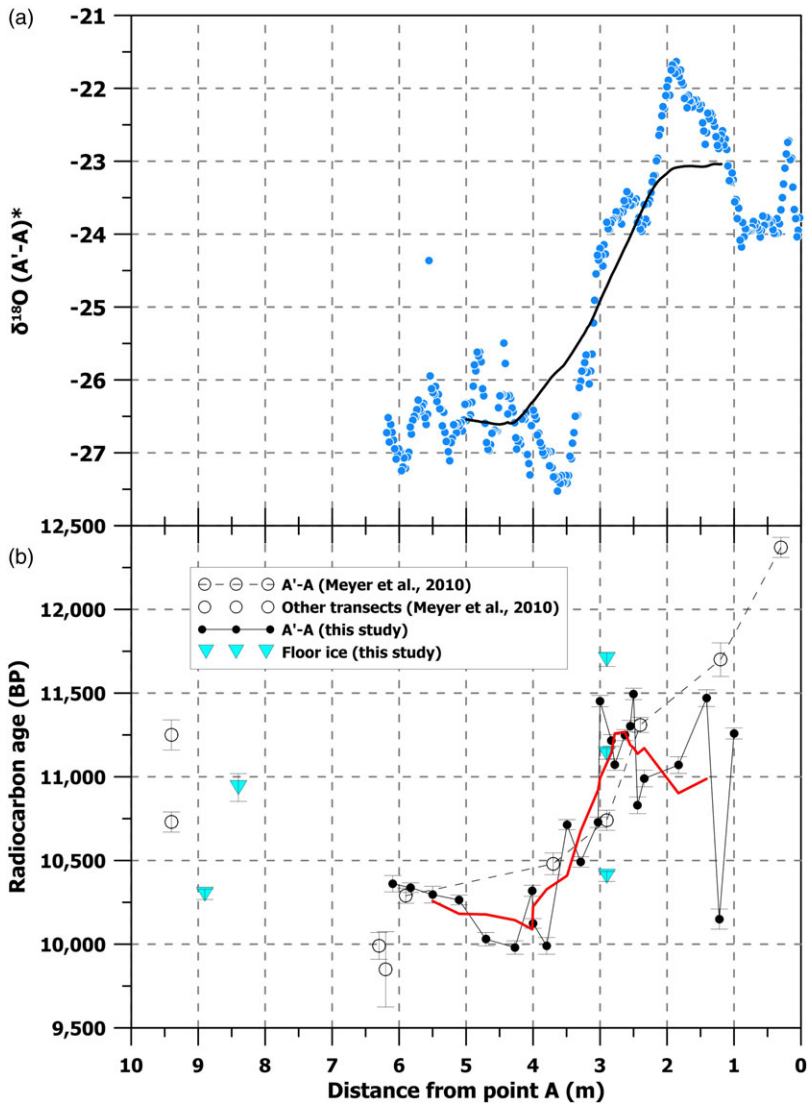


Figure 3 (a) Profile of oxygen stable isotope ratios (blue dots) along transect A'-A (from Iizuka et al. 2019, as indicated by an asterisk). The solid line is the running mean; (b) Radiocarbon ages of the macro-plant remains from the massive ground ice sampled in the Barrow Permafrost Tunnel. Error bars indicate  $2\sigma$  measurement uncertainty. The solid red line is the running mean of radiocarbon ages by this study along A'-A.

(Meyer et al. 2010a). Radiocarbon dating by Meyer et al. (2010a) indicates that sediments in Unit II were deposited Mid to Late Wisconsin age. Other radiocarbon dates indicate that the Barrow unit near Utqiagvik was deposited during the Mid-Wisconsin Interstade (about 25–40 ka BP) when the Woronzofian Transgression affected the coastal area of Utqiagvik (Brown 1965; Hopkins 1973; Sellman and Brown 1973). The time range of the Simpsonian (53–81 ka BP) and Woronzofian (25–40 ka BP) transgressions could be contemporary with the period between MIS 5a/c and MIS 3, when global sea level was 50 m or lower than today.

The large age unconformity between massive ground ice and upper Unit II indicates that penetration of ice-wedging reached the depth of Unit I, and that most of the older deposits before Unit II developed were removed from the space of the entire tunnel length. Relatively younger ages of plant remains at the bottoms of G5 (36 ka BP) and CB1 (40 ka BP) may be remnants from Unit II sediments.

On the other hand, it is worth noting that our results show that the age unconformity between the massive ice and the underlying old sediments extends more than 7 m (between Boreholes G4 and CB1) along the tunnel length (Figure 2). The westernmost (left-end in Figure 2) borehole G4 is located towards the edge of the massive ground ice. The boundary depth between massive ice and underlying sediment is the highest (about 5.2 m) compared with the lowest boundary at CBIW (about 7 m). This fact suggests that the shape of the boundary between Unit I and Unit II coincides with the shape of the ice-wedge outline formed by penetrations of winter cracking. If the ice in the tunnel wedged into Unit II (assuming it was a spatially uniform stratified deposition), we expect the oldest age in the sediments beneath the bottom (the deepest penetration point) of the ice wedge and the younger age towards the ice-wedge rims. However, we could not find a clear age shift in the sediments immediately below the ice wedge. Rather, we found ages older than 50 ka BP in the sediments beneath the deepest ice-wedge penetration (CBIW) and the shallowest location (G4) towards the ice-wedge rim. Our results are the first comparison of sediment ages in a long profile just below massive ground ice interpreted as an ice wedge.

The large age gap between ice and sediment even at the higher ice wedge rim (G4) could be explained in various ways. The first possibility is that Unit I, sedimented from about 7 m below (at the bottom of CBIW), was dislocated upwards by thrusting while the lateral ice growth pushed the adjacent sediment sideways. However, observations documenting an upward sediment dislocation of 1.8 m by ice-wedge thrusting have not been reported (to our knowledge), making this explanation seem unlikely. Differential frost heave to dislocate the lower and older sediment upward by 1.8 m also appears unreasonable considering the epigenetic ice-wedge formation processes and the presence of unfrozen saline permafrost in Unit I. We thus considered another possibility.

Assuming that the uncalibrated (calibrated) radiocarbon ages of plant remains in the sediments (Figure 2 and Table 1) represent sedimentation ages of the sample locations, we can calculate sedimentation rates for lower and upper Unit II to be 41–152 mm/uncal ka (49–155/cal ka) and 58 mm/uncal ka (47 mm/cal ka), respectively. In this calculation, we used the sample depth of the 21,670 BP as the boundary of upper and lower Unit II. For the lower Unit II, ages from the sediments at G4 and CB1 were used. The sedimentation rates for lower and upper Unit III are 5556 mm/uncal ka (3,049 mm/cal ka) and 89 mm/uncal ka (76 mm/cal ka), respectively. The sedimentation rates of Unit III (the rate of upper Unit III includes the sedimentation of the bottom portion of Unit IV) were based on the three ages from the Unit III/IV sediment by Meyer et al. (2010a), using the depth of 9930 BP as the boundary of upper and lower Unit III. The slow sedimentation rate of Unit II can be attributed to the dry and cold climate during the late Pleistocene, and the significantly faster sedimentation of the lower Unit III is probably due to alluvial or fluvial activities in a warmer climate in the Early Holocene.

We can thus consider It is also reasonable attributing the large age gap and the slow sedimentation rate of Unit II to some geological event that eroded a significant amount of the surface materials prior to ice-wedge formation, such as river flooding, pro-glacial lake outburst

flooding, pluvial flooding, or groundwater flooding. Although more work, beyond the scope of this paper, is needed to distinguish between various hypotheses, the broad distribution of the age gap between massive ice and underlying sediments appears to support the hypothesis of an erosional event. Sediments about 0.2 m below the ice mass at Borehole CB1 (7 m depth) contained numerous tree and shrub pollen (*Picea*, *Pinus*, *Betula*, and *Alnus*) and were regarded as reworked materials by Meyer et al. (2010a). High proportions of reworked pollen were also reported for Units I and II. However, an aerial transport origin of those reworked materials that could cause the age gap at the bottom of the massive ground ice cannot be excluded. If some erosional events indicated by the ages of the ice wedge-sediment boundary had occurred, these events date to about 12–36 ka BP (14–41 cal ka BP). The 12 ka BP (12,370 BP) is the oldest age from the massive ice (Meyer et al. 2010a), and the 36 ka BP (36,370 BP) is the earliest age at the top of the underlying sediment layer from this study. The age range of 12–36 ka BP falls into the Woronzofian transgression (MIS 3).

### Radiocarbon Dating of Densely Sampled Massive Ground Ice

We sampled a substantial number (29) of plant remains for radiocarbon dating from the massive ground ice in the tunnel floor and along the A'-A line (about 6.2 m) (Table 1). The overall trend of the radiocarbon ages of these plant remains followed the findings of Meyer et al. (2010a). The general trend is that the central portion of the ice contained the youngest plant remains at around 6 m from Point A (eastern edge of the tunnel). The age became older towards both ends of the tunnel (Figure 3). However, our high-resolution sampling revealed several age inversions inconsistent with the ice-wedge formation as a mechanism of the massive ice formation along the transect A'-A. Our results also show a significant fluctuation up to about 1.5 ka along the semi-horizontal transect of the massive ground ice. In permafrost environments, the decomposition rate of live plants or detritus is slow due to the low temperature, and they could be preserved in frozen ground for extended periods. Old organic matter can be easily introduced into a certain sedimentation layer, causing age inversions, known as the “old carbon problem” or “reservoir effect” (e.g., Nelson et al. 1988; Charman and Garnett, 2005; Schuur et al. 2009). Substantial inversions in radiocarbon ages of organic matter in a single wedge ice have also been reported in other permafrost regions (e.g., Opel et al. 2011; Lachniet et al. 2012; Wetterich et al. 2021).

The radiocarbon ages of plant remains in the massive ground ice along the vertical profile in Borehole G3 ranged from 10.3 to 11.6 ka BP with inversions of up to 1 ka (Figure 4). This magnitude of age fluctuation is comparable to the range found along A'-A transect. Apparent relationships between stable water isotope ratios and radiocarbon ages were not found (Figure 4).

Allowing the age uncertainty due to the old carbon problem, the newly obtained dense age profile along A'-A can be treated as a step change from the older age range (around 11–11.5 ka BP at 1.0–3.0 m) to the younger range (around 10–10.5 ka BP at 3.8–6.2 m). The oxygen stable isotope ratio dropped from around  $-23$  to  $-26.5$  ‰ at the location of the step change in radiocarbon ages (from 3.0 to 3.8 m; Fig 3). The interval of 3.0–3.8 m also coincides with an anomalous increase of methanesulfonate ion concentration found by Iizuka et al. (2019), indicating increased openings in the nearby ice-covered sea surface. This step-wise distribution of radiocarbon ages of plant remains and coinciding geochemistry in the massive ground ice can be explained by intermittent ice wedge growth. The ice portions of 1.0–3.0 m and 3.8–6.2 m in A'-A were formed by the ice-wedge mechanism during 11–11.5 ka BP and 10–10.5 ka BP,

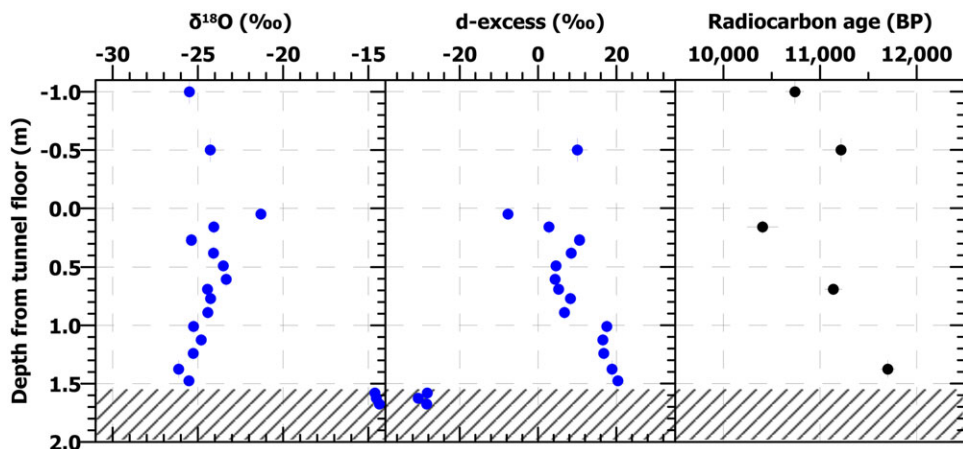


Figure 4 Vertical profiles of stable water isotope ratios and radiocarbon ages of the macro-plant remains sampled from Borehole G3. Vertical bars indicate sample lengths. Horizontal error bars for radiocarbon age indicate  $2\sigma$  measurement uncertainty. The profiles of stable water isotopes are from Iwahana et al. (2021).

respectively, during which the cracking and surface water/plant infiltrations occurred in more random locations than the classical ice-wedge growth model.

This step-wise change can also be attributed to sampling geometry against the three-dimensional ice-wedge configuration. According to Figure 4 in Meyer et al. (2010a), which shows an inferred top view of the ice-wedge system of the tunnel, the massive ice portion from 3.0 to 6.2 m is located in the area where two ice wedges merge. The profile from 0 to 3.0 m follows the direction of an ice-wedge growth, while the sampling direction of the ice portion from 3.0 to 6.2 m gradually aligns with the central line of the other ice wedge, which should have similar ice chemistry and ages of included plant remains. This possible sampling-line misalignment may have also caused the large age fluctuations along Borehole G3 (Figure 4). Otherwise, introducing unknown growth mechanisms for the massive ground ice of the Barrow Permafrost Tunnel may be required.

## SUMMARY AND IMPLICATIONS

Plant remains collected from the topmost sediment layer beneath the massive ground ice in the Barrow Permafrost Tunnel were dated as older than the radiocarbon dating limit. A significantly large radiocarbon age gap was found between plant remains in the massive ground ice (10–12 ka BP) and the topmost sediments (36 ka BP or older) of the underlying layer. Our confirmation of the age gaps (more than 24 ka) throughout at least a 7-m profile of the massive ground ice bottom could be attributed to the dislocation of the lower and older sediment layer due to upward thrusting at the boundary between ice and sediments while the growing ice wedge pushed the sediment sideways. Alternatively, the age gap indicates large-scale erosional events that removed the ground surface from the site before the development of Unit II with the massive ground ice at about 12–36 ka BP (14–41 cal ka BP).

Our dense sampling and radiocarbon dating of plant remains in the massive ground ice along the semi-horizontal profile in the tunnel showed several inversions and fluctuations up to about 1.5 ka within the profile. While the overall trend of the age change in the horizontal profile of

the massive ice supported the ice-wedge hypothesis as the mechanism of the massive ice formation, the age resolution of the information that could be retrieved from the ice wedge might be coarser than that estimated from the previous studies considering the age inversions found in this study. Our dense radiocarbon dating of plant remains in the massive ground ice can also be interpreted as a step-wise change in the ages from one portion to another of the massive ground ice mass that coincides with a similar step-wise change in stable water isotopes. These newly interpreted distributions of the geochemistry and ages of plant remains in the massive ground ice can be explained by intermittent ice-wedge growth, a possible misalignment between sampling direction and the ice-wedge growth line, or else require the introduction of unknown processes of the ice mass development.

## ACKNOWLEDGMENTS

The Ukpeaġvik Iñupiat Corporation (UIC) science team, Jerry Brown, Craig Tweedie, and Kenji Yoshikawa, have maintained conditions of the Barrow Permafrost Tunnel for scientific use and kindly supplied logistical support. This work was supported by the Environment Research and Technology Development Fund (2-1605), the Gordon and Betty Moore Foundation grant (GBMF5488), and NASA ABoVE (Arctic Boreal and Vulnerability Experiment (NNX17AC57A)).

## REFERENCES

- Boereboom T, Samyn D, Meyer H, Tison JL. 2013. Stable isotope and gas properties of two climatically contrasting (Pleistocene and Holocene) ice wedges from Cape Mamontov Klyk, Laptev Sea, northern Siberia. *The Cryosphere* 7(1):31–46. doi: [10.5194/tc-7-31-2013](https://doi.org/10.5194/tc-7-31-2013)
- Brigham-Grette J, Hopkins DM. 1995. Emergent marine record and paleoclimate of the last interglaciation along the northwest Alaskan coast. *Quaternary Research* 43(2):159–173. doi: [10.1006/qres.1995.1017](https://doi.org/10.1006/qres.1995.1017)
- Brown J. 1969. Ionic concentration gradients in permafrost Barrow, Alaska. Hanover, NH, USA: Cold Regions Research and Engineering Laboratory CRREL Research Report No.: 272.
- Brown J. 1965. Radiocarbon dating, Barrow, Alaska. *Arctic* 18(1):36–47. doi: [10.14430/arctic3448](https://doi.org/10.14430/arctic3448)
- Brown J, P. C. Miller, L. L. Tieszen, F. L. Bunnell. 1980. An arctic ecosystem—the coastal tundra at Barrow, Alaska. Stroudsburg, Pennsylvania: Dowden, Hutchinson, and Ross, Inc. (US/IBP Synthesis series).
- Carter LD, Brigham-Grette J, Hopkins DM. 1986. Late Cenozoic marine transgressions of the Alaskan Arctic Coastal Plain. In: Heginbottom JA, Vincent JS, editors. Correlation of Quaternary deposits and events around the margin of Beaufort Sea: Geological Survey of Canada Open-File Report 1237. p. 21–26.
- Charman DJ, Garnett MH. 2005. Chronologies for recent peat deposits using wiggle-matched radiocarbon ages: problems with Old Carbon contamination. *Radiocarbon* 47(1):135–145. doi: [10.1017/S0033822200052255](https://doi.org/10.1017/S0033822200052255)
- Colangelo-Lillis J, Eicken H, Carpenter SD, Deming JW. 2016. Evidence for marine origin and microbial-viral habitability of sub-zero hypersaline aqueous inclusions within permafrost near Barrow, Alaska. *FEMS Microbiology Ecology* 92(5):fiw053. doi: [10.1093/femsec/fiw053](https://doi.org/10.1093/femsec/fiw053)
- Cooper ZS, Rapp JZ, Carpenter SD, Iwahana G, Eicken H, Deming JW. 2019. Distinctive microbial communities in subzero hypersaline brines from Arctic coastal sea ice and rarely sampled cryopegs. *FEMS Microbiology Ecology* 95(fiz166). doi: [10.1093/femsec/fiz166](https://doi.org/10.1093/femsec/fiz166). [accessed 2021 Jan 19]. <https://doi.org/10.1093/femsec/fiz166>
- Dinter DA, Carter LD, Brigham-Grette J. 1990. Late Cenozoic geologic evolution of the Alaskan North Slope and adjacent continental shelves. In: Grantz A, Johnson L, Sweeney JF, editors. *The Arctic Ocean Region*. Vol. L. Geological Society of America. p. 459–490.
- Farquharson L, Mann D, Rittenour T, Groves P, Grosse G, Jones B. 2018. Alaskan marine transgressions record out-of-phase Arctic Ocean glaciation during the last interglacial. *Geology* 46(9):783–786. doi: [10.1130/G40345.1](https://doi.org/10.1130/G40345.1)
- Gilbert GL, Kanevskiy M, Murton JB. 2016. Recent advances (2008–2015) in the study of ground ice and cryostratigraphy. *Permafrost and Periglacial Processes* 27(4):377–389. doi: [10.1002/ppp.1912](https://doi.org/10.1002/ppp.1912)
- Hopkins D. 1967. Quaternary marine transgressions in Alaska. In: *The Bering Land Bridge*. International Association for Quaternary Research. p. 495.

- Hopkins DM. 1973. Sea level history in Beringia during the past 250,000 years. *Quaternary Research* 3(4):520–540.
- Iizuka Y, Miyamoto C, Matoba S, Iwahana G, Horiuchi K, Takahashi Y, Kanna N, Suzuki K, Ohno H. 2019. Ion concentrations in ice wedges: an innovative approach to reconstruct past climate variability. *Earth and Planetary Science Letters* 515:58–66. doi: <https://doi.org/10.1016/j.epsl.2019.03.013>
- Iwahana G, Cooper ZS, Carpenter SD, Deming JW, Eicken H. 2021. Intra-ice and intra-sediment cryopeg brine occurrence in permafrost near Utqiagvik (Barrow). *Permafrost and Periglacial Processes* 32(3):427–446. doi: <https://doi.org/10.1002/ppp.2101>
- Lachenbruch AH. 1962. Mechanics of thermal contraction cracks and ice-wedge polygons in permafrost. *Geological Society of America GSA Special Papers*.
- Lachniet MS, Lawson DE, Sloat AR. 2012. Revised <sup>14</sup>C dating of ice wedge growth in interior Alaska (USA) to MIS 2 reveals cold paleoclimate and carbon recycling in ancient permafrost terrain. *Quaternary Research* 78(2): 217–225. doi: [10.1016/j.yqres.2012.05.007](https://doi.org/10.1016/j.yqres.2012.05.007)
- Leffingwell E de K. 1915. Ground-ice wedges: the dominant form of ground-ice on the north coast of Alaska. *The Journal of Geology* 23(7): 635–654. doi: [10.2307/30062549](https://doi.org/10.2307/30062549)
- Mackay JR. 1974. Ice-wedge cracks, Garry Island, Northwest Territories. *Canadian Journal of Earth Sciences* 11(10):1366–1383. doi: [10.1139/e74-133](https://doi.org/10.1139/e74-133)
- Mackay JR. 1990. Some observations on the growth and deformation of epigenetic, syngenetic and anti-syngenetic ice wedges. *Permafrost and Periglacial Processes* 1(1):15–29. doi: <https://doi.org/10.1002/ppp.3430010104>
- Meyer H, Opel T, Laepple T, Dereviagin AY, Hoffmann K, Werner M. 2015. Long-term winter warming trend in the Siberian Arctic during the mid- to late Holocene. *Nature Geosci.* 8(2):122–125. doi: [10.1038/ngeo2349](https://doi.org/10.1038/ngeo2349), <http://www.nature.com/ngeo/journal/v8/n2/abs/ngeo2349.html#supplementary-information>.
- Meyer H, Schirmermeister L, Andreev A, Wagner D, Hubberten H-W, Yoshikawa K, Bobrov A, Wetterich S, Opel T, Kandiano E, et al. 2010a. Lateglacial and Holocene isotopic and environmental history of northern coastal Alaska—results from a buried ice-wedge system at Barrow. *Quaternary Science Reviews* 29 (27–28):3720–3735. doi: [10.1016/j.quascirev.2010.08.005](https://doi.org/10.1016/j.quascirev.2010.08.005)
- Meyer H, Schirmermeister L, Yoshikawa K, Opel T, Wetterich S, Hubberten H-W, Brown J. 2010b. Permafrost evidence for severe winter cooling during the Younger Dryas in northern Alaska. *Geophysical Research Letters* 37: L03501. doi: [10.1029/2009gl041013](https://doi.org/10.1029/2009gl041013)
- Nelson RE, Carter LD, Robinson SW. 1988. Anomalous radiocarbon ages from a Holocene detrital organic lens in Alaska and their implications for radiocarbon dating and paleoenvironmental reconstructions in the Arctic. *Quaternary Research* 29(1):66–71. doi: [10.1016/0033-5894\(88\)90072-5](https://doi.org/10.1016/0033-5894(88)90072-5)
- Opel T, Dereviagin AY, Meyer H, Schirmermeister L, Wetterich S. 2011. Palaeoclimatic information from stable water isotopes of Holocene ice wedges on the Dmitrii Laptev Strait, northeast Siberia, Russia. *Permafrost and Periglacial Processes* 22(1):84–100. doi: [10.1002/ppp.667](https://doi.org/10.1002/ppp.667)
- Opel T, Meyer H, Wetterich S, Laepple T, Dereviagin A, Murton J. 2018. Ice wedges as archives of winter paleoclimate: a review. *Permafrost and Periglacial Processes* 29(3):199–209. doi: [10.1002/ppp.1980](https://doi.org/10.1002/ppp.1980)
- Ramsey CB. 2009. Bayesian analysis of radiocarbon dates. *Radiocarbon* 51(1):337–360. doi: [10.1017/S0033822200033865](https://doi.org/10.1017/S0033822200033865)
- Rapp JZ, Sullivan MB, Deming JW. 2021. Divergent genomic adaptations in the microbiomes of Arctic subzero sea-ice and cryopeg brines. *Frontiers in Microbiology* 12. <https://www.frontiersin.org/articles/10.3389/fmicb.2021.701186>
- Reimer PJ, Austin WEN, Bard E, Bayliss A, Blackwell PG, Ramsey CB, Butzin M, Cheng H, Edwards RL, Friedrich M, et al. 2020. The IntCal20 Northern Hemisphere radiocarbon age calibration curve (0–55 cal kBP). *Radiocarbon* 62(4):725–757. doi: [10.1017/RDC.2020.41](https://doi.org/10.1017/RDC.2020.41)
- Schuur EAG, Vogel JG, Crummer KG, Lee H, Sickman JO, Osterkamp TE. 2009. The effect of permafrost thaw on old carbon release and net carbon exchange from tundra. *Nature* 459(7246): 556–559. doi: [10.1038/nature08031](https://doi.org/10.1038/nature08031)
- Sellman PaulV, Brown J. 1973. Stratigraphy and diagenesis of perennially frozen sediments in the Barrow, Alaska, Region. Vol. North American Contribution. National Academy of Sciences. p. 171–181.
- St-Jean M, Lauriol B, Clark ID, Lacelle D, Zdanowicz C. 2011. Investigation of ice-wedge infilling processes using stable oxygen and hydrogen isotopes, crystallography and occluded gases (O<sub>2</sub>, N<sub>2</sub>, Ar):49–64.
- Uchida M, Mantoku K, Kobayashi T, Kawamura K, Shibata Y. 2023. Ultra small mass AMS <sup>14</sup>C sample preparation and analyses at NIES-TERRA AMS facility. *Nuclear Instruments and Methods in Physics Research Section B: Beam Interactions with Materials and Atoms* 536:144–153. doi: [10.1016/j.nimb.2022.12.028](https://doi.org/10.1016/j.nimb.2022.12.028)
- Uchida M, Shibata Y, Ohkushi K, Yoneda M, Kawamura K, Morita M. 2005. Age discrepancy between molecular biomarkers and calcareous foraminifera isolated from the same horizons of

Northwest Pacific sediments. *Chemical Geology* 218(1):73–89. doi: [10.1016/j.chemgeo.2005.01.026](https://doi.org/10.1016/j.chemgeo.2005.01.026)

Wetterich S, Meyer H, Fritz M, Mollenhauer G, Rethemeyer J, Kizyakov A, Schirrmeister L, Opel T. 2021. Northeast Siberian permafrost ice-wedge stable isotopes depict pronounced last glacial maximum winter cooling. *Geophysical Research*

Letters 48(7):e2020GL092087. doi: [10.1029/2020GL092087](https://doi.org/10.1029/2020GL092087)

Zhong Z-P, Rapp JZ, Wainaina JM, Solonenko NE, Maughan H, Carpenter SD, Cooper ZS, Jang HB, Bolduc B, Deming JW, Sullivan MB. 2020. Viral ecogenomics of arctic cryopeg brine and sea ice. *mSystems* 5(3):e00246–20. doi: [10.1128/mSystems.00246-20](https://doi.org/10.1128/mSystems.00246-20)